Charles University

Faculty of Science

Study programme: Bioinformatics

Study branch: Bioinformatics

Bc. Lenka Backová

Bioinformatical analysis of the complex multidimensional microscopy datasets

Bioinformatická analýza komplexních multidimensionálních mikroskopických dat

Supervisor: Prof. RNDr. Jan Černý, Ph.D.

Bachelor's thesis

Prague 2020

I declare that I carried out this bachelor thesis independently, and only with the cited sources, literature and other professional sources. It has not been used to obtain another or the same degree.

I understand that my work relates to the rights and obligations under the Act No. 121/2000 Sb., the Copyright Act, as amended, in particular the fact that the Charles University has the right to conclude a license agreement on the use of this work as a school work pursuant to Section 60 subsection 1 of the Copyright Act.

In ..... date ....

Author's signature

Firstly, I would like to thank Prof. RNDr. Jan Černý, Ph.D., who has been nothing but supportive of my pursuit of this topic, excited for the opportunity and possibilities of our cooperation and helped me relentlessly until the last moments.

I would like to thank Mgr. Aleš Benda, Ph.D., who has taken me under his guidance, offered me a position to continue my work and has always offered his knowledge and wisdom.

Furthermore, I would like to thank RNDr. Michaela Efenberková, Ph.D. for her guidance with learning about deconvolution and her help during my SVI Huygens usage.

I would like to thank Bc. Karolína Knížková, who has shown me multiple times how she acquires her data, which she then offered me for my studies and explained to me meticulously the biology behind the data.

I am grateful for my family, for their encouragement, guidance and help.

Abstract

Microscopy is embedded in the history of life sciences and vice versa. Recent advances in the field present new challenges as new revolutionary technologies arise. Sample preparation, microscope operation and data analysis have become particularly demanding requiring specific interdisciplinary expertise. Bioimaging data analysis is computationally demanding, as microscopy technologies can easily acquire data of exceptional size, often in terabytes. Correct analysis requires computer vision knowledge, as well as knowledge of studied biological systems and last, but not least deep understanding of microscopy technology. Tools available for the analysis of the imaging data vary from open-source customizable software with a coverage of multiple tasks to a task specific proprietary software. To choose the best tools for the analysis, analysts should know their options and tasks at hand. In bioimage analysis the tasks needed to be employed depend on the desired outcome and the acquisition technology. Amongst the possible tasks to consider belong deconvolution, segmentation and registration. Amount of approaches and algorithms available is progressively growing, resulting in a complex field, difficult to be easily familiar with. This thesis covers different microscopy technologies with emphasis on light sheet fluorescence microscopy, particularly stressing the details of image acquisition and how it influences the analysis. It also reports on different approaches to main image analysis tasks and tools available, to illustrate the depth and immensity of the field.

Keywords: microscopy, big data, bioimage analysis, light sheet fluorescence microscopy, segmentation, deconvolution, 3D reconstruction, quantification of the imaging data

Abstrakt

Mikroskopia je odbor, ktorý je súčasťou biologických vied a ich histórie. Rast tohto odboru, vznik nových revolučných technológií, so sebou prináša nové výzvy. Príprava vzoriek, obsluha mikroskopu a spracovanie biologických obrazových dát sa stávajú neustále náročnejšími a vyžadujú medzidisciplinárnu expertízu špecifickú pre dané oblasti. Dnešné mikroskopické technológie generujú obrovské množstvo dát, často v terabajtoch, vďaka čomu sa analýza biologických obrazových dát stáva výpočtovo náročná. K analýze je potrebná znalosť počítačového videnia, mikroskopických technológií a skúmaných biologických systémov. K dispozícii sú nástroje v rôznorodej škále, od open-source riešení, ktoré pokrývajú veľké množstvo úkonov, k proprietárnym softwarom zameraným na jeden úkon. Analytici by sa mali orientovať v možnostiach spracovania a v úkonoch, ktoré plánujú vykonať, aby vybrali najlepšie nástroje. Úkony potrebné vykonať závisia od požadovaného výsledku a technológie, ktorá bola použitá na získanie obrazových dát. Medzi možné úkony patrí dekonvolúcia, segmentácia a registrácia dát. Neustále vznikajú nové prístupy a algoritmy na analýzu, vďaka čomu je analýza obrazových dát zložitá. Táto práca sa zaoberá rôznymi mikroskopickými technológiami so zameraním na light sheet fluorescence mikroskopiu, problematiku získavaniu snímok a ako to ovplyvňuje analýzu. Na ilustráciu rozsiahlosti oblasti analýzy biologických obrazových dát sa práca zaoberá rôznymi dostupnými prístupmi a úkonmi analýzy.

Klíčové slová: mikroskopie, big data, analýza biologických obrazových dát, light sheet mikroskopie, segmentace, dekonvoluce, 3D rekonstrukce, kvantifikace obrazových dát

Contents

Introduction

The field of microscopy has been developing for four centuries. For the last almost one and half century the light microscopy have been thought to be limited in the resolution by physical principles, eg. Abbe's diffraction limit. In the last two decades we can witness several optical technologies breaking diffraction-based limitations, such as Stimulated Emission Depletion (STED) technology [1], Photo-activated localization microscopy (PALM) or Single Molecule Loclization Microscopy (SMLM) principle. Recent advances in light microscopy have materialized in novel super-resolution microscopy, virtual slide microscopy, light-sheet microscopy, novel sample preparation and labelling approaches and many others. Electron microscopy, which uses electron beams to obtain high resolution images does not stand behind. Generally speaking, recent advances have been made to diminish noise, artefacts and aberrations during or after image acquisition, which led to Nobel prize for cryogenic electron microscopy (cryo-EM) in 2017. On top of that light and electron microscopy can be combined (CLEM) to get the best out of the two approaches.

Currently big data have become a challenging part of data analysis in many different fields, life sciences and physics, agriculture, or economics. Challenges big data bring to the scene are various. Storing recent data is more costly, computation time is longer, requirements for computation hardware are increasing and traditional algorithms or tools may not be efficient enough, thus becoming obsolete.

Imaging biological samples in higher resolution comes with long acquisition times and large file sizes. Images from multiple types of microscopes are now imaged in z-stacks, thus providing information in three dimensions, instead of just two. Furthermore, live cell time-dependent imaging adds another dimension to the dataset, increasing imaging time, size of the dataset, computation time and the requirements for visualization abilities.

Bioimage analysis is very complex field as different approaches have to be applied to analyse particular microscopy images. Analytical demands differ based on the desired outcome of the experiment and as the field of image data mining grows the complexity of the tasks increases. Microscopy also requires a high level of interdisciplinarity. To understand the underlying technologies applied and meaning of the results obtained, it is necessary to combine biology with physics, chemistry and computer science as well [2].

Bioimage data analysis comprises of several different tasks including enhancement of the quality of data or detection of cells or organelles. Image pre-processing focuses on quality of the raw data, signal-to-noise ratio, resolution or detection of artefacts in the acquired image. Subsequent quantitative analysis focuses on quantifying imaged data, measuring distances between objects or their sizes, counting cells or organelles, tracking the development and movement of cells, or finding ratio of an organelle, object or dye in the whole volume.

I got recently involved in different tasks in bioimage data analysis focusing on images acquired applying Light Sheet Fluorescence Microscopy (LSFM). These tasks include image registration, deconvolution, segmentation and further quantitative analysis. We examine different algorithmic approaches, as well as different

commercial or open-source software for data analysis. The purpose of this thesis is to give an overview of available technologies and options in microscopy, different approaches and tasks in data analysis and to illustrate the varying challenges amongst which are the computation and storage requirements, as one could underestimate their importance in the microscopy field.

1. Microscopy

In a very general way microscope uses a beam to illuminate the observed sample to project the magnified image of the object onto the eye retina of the observer or the detection device. The device detects the spatially resolved intensity of the signal and forms the image.

1.1 Types of Microscopy

There are many different types of microscopes, which will be briefly described to showcase the variety of the imaging field.

1.1.1 Optical and electron microscopy

Microscopes are distinguished into two main groups: optical (often referred to as light) and electron microscopes. There exist another groups, for example scanning probe microscopes, that use probes to scan the surface of an object and record properties or shapes of its surface, amongst which belongs atomic force microscope or scanning near-field optical microscope.

Optical microscopy

Optical microscopes use light as a source of illumination to visualize the observed object. Often light from the visible spectrum is used, for fluorescence microscopy wider wavelength range of illumination source may be used, extending from UV (ultraviolet) to NIR (near-infrared). To achieve image magnification convex lenses are used. Compound microscopes use multiple lenses [3].

A setup of an optical microscope may be the finite tube length or infinity optics microscope, the difference is the plane, at which the lenses project the image. In the finite tube length microscope, there are two lenses - objective and ocular lens in the microscope. Objective lens is at a working distance from the sample and forms a magnified, real image at the intermediate image plane. The intermediate image plane is fixed and occurs in the focal plane of the ocular. As the image is located at the focal length of the ocular lens, the image is further magnified and projected into infinity, which then forms a real image when observed by eye. In the infinity optics microscope, the objective lens projects the image into the infinity and the real image is formed at the intermediate image plane by a tube lens in the body of the microscope. Objectives are usually made from different lenses with different properties, depending on to what extent are they corrected for various aberrations. Modern microscopes have multiple accessories available and thus the light can travel in more than one pathway - to the ocular or to the specialized digital detectors [4].

The wide-field detector is mounted on the microscope. The surface, which detects light signal, is placed at the intermediate image plane or at the projected image of the intermediate image plane. The photosensitive surface may be a CCD (charge-coupled device) or sCMOS (scientific Complementary Metal Oxide

Semiconductor) chip. The chip has a grid of photosensitive pixels, which simultaneously capture light signal from the object. Each pixel captures the light signal (a number of photons incident on the pixel) as a charge, which is converted to analogue voltage, which is further converted to a digital number.

Electron microscopy

Electron microscopes use beam of accelerated electrons as a source. Electrons are emitted from a cathode, accelerated by a high voltage, beam is then focused and lands on the sample. Electron microscopy requires vacuum for a proper function. Electron microscopy is introduced in more depth in [5].

There are two main types of electron microscope: transmission (TEM) and scanning (SEM). In TEM the electrons pass through the sample and the imaging happens in pass-through mode, whereas in SEM imaging is made from scattered electrons or emitted X-rays. In TEM electrons are transmitted through very thinly sliced object, and the contrast comes from the interaction of the object with electrons.

In SEM one can observe multiple characteristics of the target object based on the type of detector used. A detector of backscattered electrons detects high-energy electrons scattered elastically from the object. Heavy atoms reflect more electrons, hence position with heavier atoms is brighter in the image. Detector of secondary electrons detects low-energy electrons, which originated by inelastic scattering of electrons by being ejected from valence band of the object atoms. These electrons carry information about the topology of the surface, where areas perpendicular to the electron beam are less intense. X-ray spectroscopy may be added to evaluate, which elements are present in the object, seldom used in life science. With their high magnification and high resolution electron microscopes produce relatively large data, namely when combination of several probes is applied (correlation with fluorescence, element analysis or spectroscopy) or imaging is performed in 3D.

1.2 Fluorescence microscopy

In life sciences the ability to image specific molecules or different components of a specimen is very desirable. The high specificity could fulfil fluorescence microscopy.

1.2.1 Fluorescence

Fluorescence and phosphorescence are types of luminescence. Luminescence occurs after a valence electron is excited to a higher energy state. It exhibits as an emission of light. Rate of fluorescence is fast at 10^8 s^{-1} as the return of excited electron is spin-allowed, whereas rate of phosphorescence is much slower (range of $10^3 - 10^0$ s^{-1}), however light may not be emitted at all, instead radioactive decay or quenching processes occur [6]. Fluorophores are molecules, which can emit light upon absorption of energy.

After the molecule absorbs energy, it is excited to a higher energy level. Usually energy from a light source is used as opposed to thermal energy from heat

induction [6]. Light absorbed by the molecule has energy equal to the difference between energy of the ground state and the higher energy state. Substances can be characterised by their absorption and emission spectra as seen in Figure 1.1. These spectra are plots of the light intensity emitted in respect to their wavelength.

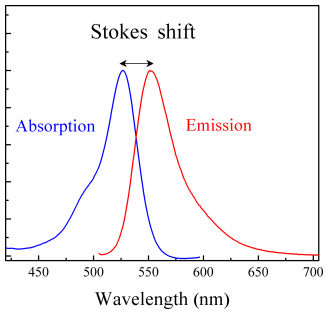

Figure 1.1: Normalised absorption and emission spectrum of rhodamine 6G showcasing Stokes shift.[2]

Jabłoński diagrams (Figure 1.2) are used to depict the processes between absorption and emission of light. Horizontal lines represent energy states and vertical lines represent transitions [6].

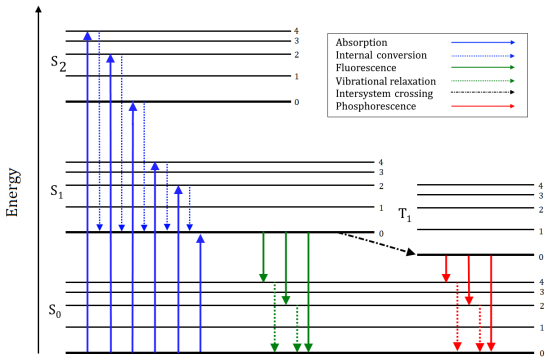

Figure 1.2: Theoretical example of Jabłoński diagram.

When fluorescent molecules absorb light, they are excited to a higher energy state S_1 or S_2. As energy states have multiple vibrational levels, excitation usually occurs to a higher vibrational level. Afterwards, process called internal relaxation occurs, during which molecules relax to the lowest vibrational energy level of the state S_1. Then, the molecule returns to the ground state and photon is emitted [6].

Typical emission spectrum is a mirror image of absorption spectrum from state $S_0 \rightarrow S_1$, as a result of the similarity between the vibrational structure of the molecule. Spacing between vibrational energy levels of the excited singlet states is similar to the spacing of the ground state, as the structure of nuclei is not altered by excitation [6].

The emission spectrum usually does not depend on the excitation wavelength, as the excess energy used to excite the molecule to the higher energy level is

[2]Courtesy of wikipedia.org

dissipated when the molecule relaxes to the lowest vibrational energy level of S_1. Thus, emission spectra usually only depict emission of light when the transition from the lowest vibrational energy level of S_1 occurs. Some compounds can emit light when a transition from state S_2 to the ground state occurs [6].

As shown in Figure 1.2, energy absorbed by the molecule is higher than the emitted energy, thus the wavelength of the absorbed light is shorter than that of the emitted light. This is called Stokes' Shift [6] and it is caused by losses of energy during fluorescence.

Fluorophores

Fluorophores are used in fluorescence microscopy as probes or dyes, as most of the molecules in the imaged cells are not very fluorescent. Specific labels for selected molecules can be targeted in the experiment [7]. The fluorophores are often aromatic molecules, amongst which belong certain proteins (Green Fluorescent Protein, Yellow Fluorescent Protein, etc.), quinine, rhodamine, and other compounds. Before use of particular fluorophores, many characteristics need to be considered, such as emission and excitation wavelength, excited state lifetime, Stokes' shift and more [6].

Green fluorescent protein is derived from a naturally occurring protein in a jellyfish *Aequorea victoria*. It is used in many imaging experiments, as the protein is expressed by a genetically modified imaged specimen and there is no need to add any external organic dyes to the biological system. Gene encoding GFP may be incorporated in to the genome in multiple ways, it may be fused to a gene for another protein as a protein tag to study gene expression [8, 9]; or it may be incorporated to a protein expressed in a specific compartment of the cell [9]. Many other fluorescent proteins have been derived and are used widely in fluorescence microscopy, overview of important characteristics of numerous fluorescent proteins is in [10].

DAPI is widely used fluorescence dye or a probe. It has a high affinity to double-stranded DNA and binds to AT-regions in the minor groove [11, 12]. Thus, the molecules after staining the tissue are located in the cell nuclei (may be in mitochondria or chloroplasts as well). DAPI can be used for chromosome staining or nuclei visualization, which can be used to count cells [13].

1.2.2 Fluorescent microscopy

Fluorescence microscopes employ excitation light to illuminate the sample, which excites the fluorophores and leads to light emission. Intensity of the emitted light is detected. Image is then acquired as assigning each position the intensity from the detector.

Fluorescence microscope must contain multiple filters, which transmit only narrow range of wavelengths and block all other wavelengths. Through the excitation filter only specific excitation wavelength passes through to reach the dichroic mirror, which directs the light towards the objective lens and thus the sample. Fluorophores in the sample are excited and upon deexcitation, they emit light. Emitted light, which is of a longer wavelength than the excitation wavelength due to Stoke's shift [14, 6], is transmitted through the dichroic mirror to the emission filter and reflected excitation light is directed towards the

light source. Emission filter blocks residual reflected excitation light and lets the emitted light pass through.

Wide-field vs. confocal

To capture the image, two main acquisition setups could be applied. Either the whole scene can be captured at once with a camera in a wide-field mode, or a point scanning mode may be used, where the signal originates from a certain small position and by changing the observed position, the whole image is then scanned and collected.

Wide-field microscopes illuminate the whole sample. Fluorescence signal from excited fluorophores in the focal plane is detected, however light emitted from out-of-focus planes is detected as well. For thick samples wide-field microscopy is not optimal, as blurry low-contrast images are produced.

Point scanning microscopes, mainly confocal microscopes, do not detect signal from the whole plane in the sample at once. The sample is illuminated by a focused laser beam (point light source) at a specific plane. The light is then collected through a pinhole, which is employed to collect light only from the correct in-focus plane and specific position in the plane [14]. The whole focused planes is scanned and a 2D image is created. The focal plane position can be changed and another plane could be imaged. This method reduces signal from out-of-focus planes. However, the pinhole also partially blocks the focal plane signal and the detected intensity of light collected is reduced. Fluorophores in the out-of-focal planes are still photobleached and the scanning process is slower than wide-field acquisition.

Epifluorescence

Imaging by fluorescence microscope often uses epifluorescence principle, where the sample is excited by an illumination source passing through the same objective as the emitted light that is detected. Such microscopes must employ dichroic mirror and filters to illuminate the object by the correct light and to detect the right signal, not the excitation light.

One-photon vs. two-photon

In the above described microscopes, it has been assumed that the fluorophores are excited by one photon of energy E, which corresponds to the energy needed to excite valence electron to a higher state. The energy E corresponds to the wavelength λ by $E = \frac{hc}{\lambda}$, where c is the speed of light and h is the Planck's constant. However, the electron may be excited by two photons with half of the energy E, if they are absorbed nearly simultaneously [14].

The hardware for the two-photon microscope tends to be more expensive, thus it should offer some improvements to justify the increased price. It has been shown that it reduces out-of-the focal -plane bleaching of the fluorophores. It also increases imaging depth and cell viability. These effects have been shown to depend on used wavelength of the laser [15].

1.3 Microscopy shortcomings

Microscopy is a complex field, which brings non-trivial challenges and problems. Microscopy images are only as good as the sample, the technology, the setup, the user and the settings. No image is a perfect representation of the real magnified sample, as it may be distorted in multiple ways.

There are multiple parameters we have to optimize for each acquisition: magnification, resolution and signal-to-noise ratio (SNR). Magnification is a ratio between the real size of the object and the imaged size. Highest magnification in the order of hundred thousand can be achieved by using electron microscopy, especially TEM. Resolution is the smallest distance between two points, which are still recognizable as two points. Both of these parameters are impacted by the wavelength of the illumination source used. Signal-to-noise ratio is a ratio of imaged signal to the background noise and can be approximated by multiple algorithms or by visual inspection. Excellent quality of image is considered for SNR around 40, acceptable is around 10.

The main degradation of image quality is convolution. Convolution is a mathematical operation noted with $*$, defined as a mapping of two functions f and g, which creates a third one as:

$$(f * g)(t) = \int_{-\infty}^{\infty} f(\tau)g(t-\tau)d\tau.$$

Resulting function carries the information, how the shape of one function is modified by the other. In microscopy the resulting image I is the convolution of the imaged object O and point spread function (PSF): $I = O * PSF$. PSF is a function, which expresses how microscope distorts a point light source observed by a microscope as a result of diffraction and various abberations. Diffraction originates from the interaction of light and objects and is the distortion of beam of light [3]. For example, light incident on an edge of an object seems to bend behind the edge and some light illuminates geometric shadow [14]. Diffraction is caused by the wave properties of light. In a microscope this originates from light passing into the circular aperture through tiny hole. Point object is distorted, specific pattern, called Airy disk pattern, is created with a central spot (or a disk) surrounded by concentric rings of lowering thickness. Bright disks are maxima of intensity, numbered from the zeroth (central disk), and dark areas between bright disks are minima numbered from the first dark disk. Central disk is called the Airy disk [14, 3]. PSF is specific for a microscope and can be estimated or approximated.

Resolution limit can be derived from the theory of diffraction and PSF. There are multiple limits, which can estimate the lowest possible resolution, amongst which are Abbe's limit and Rayleigh criterion. Rayleigh criterion is derived from the assumption, that two point light sources are still distinguishable, if the zeroth maximum of PSF of the first point is exactly in the first minimum of the PSF of the second point. Resolution limit d can be mathematically derived as:

$$d = 1.22\frac{\lambda}{2NA},$$

where λ is the wavelength of detected light, NA is the numerical aperture. Numerical aperture can be found as $NA = n \sin\theta$, where θ is the angle at which light is collected and n is the refractive index of the lens immersion medium. Abbe's limit d is defined as:

$$d = \frac{\lambda}{2NA}.$$

Interference of light is the addition to multiple beams of light. However, due to the wave property of light, the addition is not simple. When calculated analytically, the resulting intensity varies, based on the position of intersection of the light waves. The resulting intensity may be addition of the interfered intensities called constructive interference, their subtraction called destructive interference or any other partial combination [3]. Interference may be observed in microscopy, when light from focal plane interacts with out-of-focus plane signal.

Another major degradation of an image is caused by a random process, noise. Noise is caused either by photons or electronic devices, where photon noise is usually more dominant source, especially in modern devices [16]. Photon noise is caused by the probabilistic interpretation of quantum mechanics and the indeterminacy of observed photons. The intensity, which the sensor is observing and transforming into an image, is number of incident photons on a sensor pixel, which fluctuates even though the specimen intensity is constant. Photon noise follows Poisson distribution. Noise from electronic device can be usually assigned to heat or imperfections in the material (semiconductor) of the sensor. Device noise behaves according to Gaussian distribution. Noise distorts the image and thus is taken into consideration, when image is deconvolved, as a random element.

Furthermore, several optical aberrations can reduce imaging quality. Aberrations are caused by flaws in the optics and their quality and properties. Correctly aligned optical apparatus of the microscope leads to minimizing the aberrations. Amongst the aberrations belong chromatic and spherical aberration. Chromatic aberration is caused by dispersion, the variation of the refractive index of the lens with the wavelength of the light. Hence, different wavelengths are not focused into a single point. This aberration is noticeable at the boundaries of light and dark objects in the image, where a colourful range may be seen. As a result of chromatic aberration location of a probe may be more difficult, when using multiple probes [17]. Spherical aberration is caused by light being focused into different points by spherical lenses. Light is refracted (or reflected) differently based on the position of impact, whether light hits spherical surface off-centre or closer to the centre [17].

Phototoxicity of light applied on the specimen can be damaging to the image quality either by photobleaching of fluorophores or by decreasing cell viability (the ratio of healthy physiologically behaving cells in a sample). Bleaching of fluorophores is the loss of the ability to fluoresce [18], caused by photons inducing covalent modifications of the molecules, usually via different higher-energy molecular states, especially during the triplet state [19]. Light illumination in higher light doses leads to damage or death of cells in live cell imaging [20].

One of the downsides to using fluorescence microscopy is the autofluorescence. It is either shown as a low background signal, however it may be strong enough to impose as a viable signal from a fluorescence molecule. Amongst autofluorescent molecules are vitamin B, flavins, flavin proteins, reduced pyridine nucleotides (NADH and NADPH), fatty acids, porphyrins, uncoupled cytochromes, lipofuchsin pigments, serotonin and others [14]. Fixation of cells with aldehydes may induce autofluorescence. The strength of the signal of the autofluorescent molecule depends on excitation wavelength, cell type and the molecule [14]. In [21] has been concluded, that induced stress in bacterial and eukaryotic cells increases autofluorescence of the sample.

2. Light Sheet Fluorescent Microscope

In microscopy we are challenged with the triangle of compromise, since we cannot achieve good resolution at a high speed of data collection with low system sensitivity, as phototoxicity occurs. Light sheet microscope is one of the recently developed microscopes, which is unique for its ability to collect data in three dimensions for a longer time without afflicting much damage to the sample. That is achieved, as the microscope illuminates only one plane that is detected and collected [2], which is called optical sectioning. For high speed of data collection, wide-field detection device is used to image the whole illuminated plane. However, the speed and sectioning capabilities mean that huge data files are collected during the experiment. The challenges brought by working with light-sheet microscope are numerous and not only linked to the computational difficulties with the large data. To use LSM, new techniques need to be employed also to prepare the samples, mount them and to image them.

2.1 Setup

There exists numerous possible geometries for the LSM [2]. These geometries are offered by multiple companies, of which I will cover these:

- Carl Zeiss Microscopy
- LaVision BioTec
- Applied Scientific Instrumentation
- custom or opens-source design.

Selective-plane illumination microscope (SPIM)

The Lightsheet Z.1 from Carl Zeiss Microscopy has the setup of selective-plane illumination microscope (SPIM). It offers illumination from two sides and multiple excitation wavelengths. One thin section of the specimen is illuminated by the excitation laser with desired wavelength. Laser is focused onto a single plane in the specimen, the objective that detects the signal is placed perpendicular to the objective that excites the sample [22]. The layout can be seen in Figure 2.1. This setup allows the specimen to be rotated in the chamber and the lasers are split into two beams by a dichroic mirror, thus the specimen can be illuminated from two sides. This allows for multiview imaging in the LSFM, which can enhance the quality of the final picture. When imaged from one side of the specimen, the penetration of the beam worsens with distance passed, thus the quality of the image at the side not illuminated may not be ideal and double side illumination may help. Final stitching of all the multiview images is done by registration and fusion algorithms [22]. For signal detection there are two types of cameras, either two charge-coupled devices (CCD) or two scientific complementary metal-oxide

semiconductor (sCMOS) are used. Two cameras are useful, as two different emission wavelengths can be detected simultaneously, and the picture would be in two colour channels. The objects excited by excitation lasers may throw shadows in the illumination plane, which would produce stripes in the image. To avoid this artefact, the illumination beam uses pivoting of the plane to illuminate the objects from multiple angles and thus gets rid of the stripes and shadows. This geometry allows for long-term multi-view imaging, ideal for studying developmental processes [23]. The Lightsheet Z.1 is available in 2 laboratories in Prague, thus bigger emphasis will be put on this microscope.

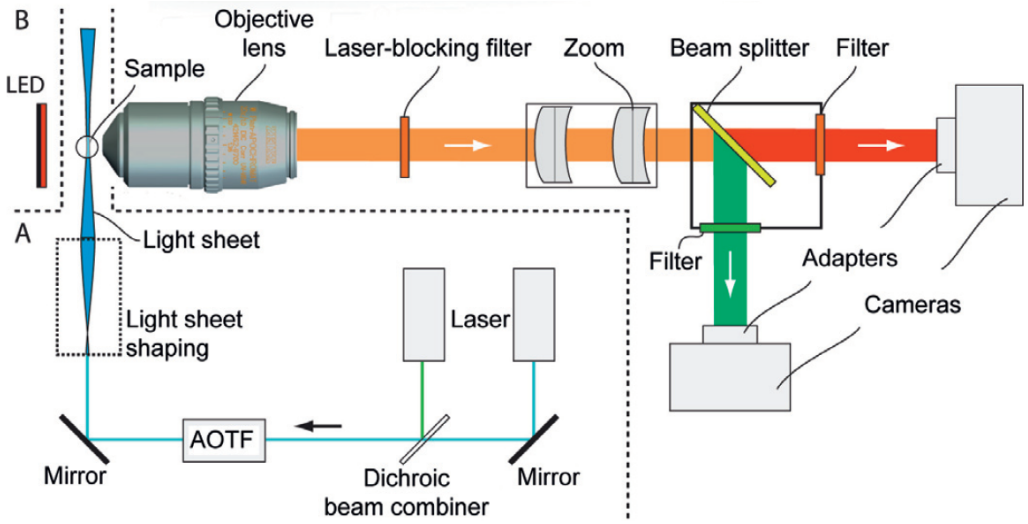

Figure 2.1: Geometry and layout of components of Lightsheet Z.1. Image taken from [22].

LaVision BioTec

Another setup is Ultramicroscope from LaVision BioTec, which was described in [24], offers uni-directional and bi-directional illumination with up to 6 illumination sheets possible from different angles [25]. Image is acquired in a wide-field mode with a sCMOS camera. To image the whole sample, it is moved in a perpendicular axis to the image plane. This setup offers great, homogenous illumination through the whole sample and therefore minimizes artefacts like stripes and shadows. Samples can be imaged intact *in vivo* or cleared after fixation, however the setup is usually recommended for cleared samples [22]. Samples are put on a dedicated platform, moved vertically and optically illuminated by horizontal sheets of light [2]. This setup is not accustomed to multiview imaging and rotation of the sample.

Applied Scientific Instrumentation

Applied Scientific Instrumentation offers components for different setups in the light-sheet microscopy domain, SPIM, iSPIM/diSPIM, oSPIM or ct-dSPIM.
Amongst the components are motorized and piezo stages, optomechanics, scanners, lasers, lenses, objectives and others. The iSPIM offers imaging on an inverted microscope and diSPIM offers dual view on an inverted microscope. The

o-SPIM is advertised to be for coverslip imaging, which generates the illumination sheet at an oblique angle and where the oil immersion objective is under the sample dish. The setup of ct-dSPIM is suitable for imaging cleared tissues in dual-view. These setups do not allow for rotation. This and further information can be found at [26].

Custom and open-source geometry

With LSFM there is an option to not obtain commercial microscope, but to build it in a lab with a custom geometry, which can be adjusted to the samples and the experiment. There exist multiple geometries described. OpenSPIM [27] is described in a great detail to instruct users to build the microscope themselves, whereas projects like OpenSPIN [28] and DIY-SPIM [29] rely on contact with the developers to build the microscopes [2, 30]. These options are more financially available and customisable, however more difficult.

2.2 Samples

Samples imaged by light sheet fluorescence microscopes can be either live or fixed. For the LSFM to be able to image them the specimen needs to be transparent, in case samples are opaque, clearing protocols have been developed. However, samples undergoing clearing have to be fixed, live imaging cannot be performed on opaque samples. Luckily, some viable biological specimens are transparent, for example zebra fish or some larvae. The Lightsheet Z.1 is good for both long-term developmental studies and cleared fixed samples. Clearing is amongst the techniques, that are now being studied extensively and customized protocols are developed for best user results. Purpose of clearing is to achieve translucence mostly extracting lipids out from the sample.

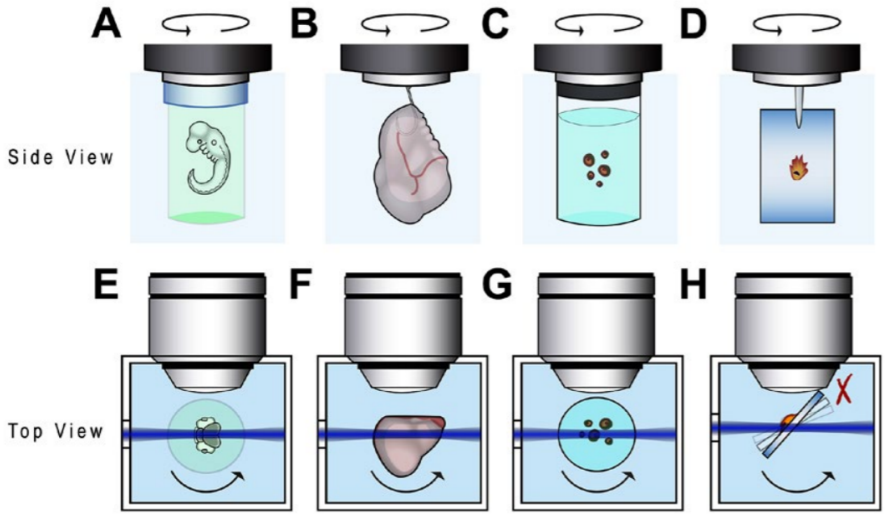

Figure 2.2: Possible ways of mounting a sample in a Lightsheet Z.1: (A) embedded in gel, (B) clipped, (C) enclosed, (D) flat (not possible in Lightsheet Z.1). (E-H) View from above on mounted samples (A-D). Picture taken from [31].

The samples can be mounted many ways depending on the desired outcome. Great benefit is the lack of the need to use coverslip for imaging, which offers whole object imaging in an easier way as the sample is not cut and it is possible to image from almost all sides. LSM also offers live imaging. Sample preparation and the sample chamber is described in [31]. In the Lighsheet Z.1 is a sample holder, which is connected to a positioning motor stage to allow for translation and rotation of the sample. Sample then can be mounted in multiple ways, it can be embedded in gel, hanging held by a hook, glued or in a capillary, on a coverslip or in a container. The mounting possibilities are shown in Figure 2.2. If embedding in gel is used, fluorescent beads may be used for multiview registration and fusion. Sample is in a chamber ideally filled with aqueous solution, however even dry sample in air can be imaged. Clearing is the process to change the refractive index of the sample without disrupting the structure of the sampled tissue and the fluorescent molecules needed for imaging. There are many techniques, using organic chemicals, aqueous solutions or electrophoretic clearing.

2.3 Data

Data from LSFM are in the form of a series of images called z-stacks, which can contain hundreds of two dimensional images. If multi-view imaging is performed, the result of this procedure is multiple z-stacks. Multiple lasers can be used during the illumination phase to excite different fluorescent molecules, resulting in multiple images of the same plane, thus multiple z-stacks. Each z-stack can be assigned different colour spectrum, which can be joined into RGB image. During time-lapse imaging, the specimen is repeatedly imaged in time intervals, consequently making large number of z-stacks. The whole imaging can last up to days due to low phototoxicity of this technology.

To acquire all the information from the specimen correct minimal sampling rate should be considered, which is derived from the Nyquist-Shannon sampling theorem. Sampling rate for image acquisition is defining the voxel size (3D pixel). Undersampling may lead to loss of signal and inability to reconstruct the original signal (object).

Nyquist rate is calculated in [32] for Lightsheet Z.1 with these parameters: $NA = 1$, excitation wavelength $\lambda_{ex} = 488$nm, emission wavelength $\lambda_{em} = 520$nm, lens immersion refractive index $n = 1.48$ and Gaussian light sheet SPIM excitation mode with the width of Gaussian light sheet $w = 11,657$. The recommended sampling rate is: $x = 130$ nm, $y = 130$ nm, $z = 464$nm. Thus, volume of a voxel is $v = x \cdot y \cdot z$. Number of voxels needed to image a sample of a volume $V = 2$ mm^3 (for example zebra fish larvae) is $n = \frac{V}{v}$. If the intensity of each voxel is stored in a byte, then size of this uncompressed dataset would be approximately 255 GB. Twice as much if two colour channels are used, and even twice as much that if dual-view.

3. Bioimage Data Analysis

Image can be described as a two dimensional set of pixels with assigned value (intensity), for example values $0 - 255$ (stored as a byte), which can be viewed as a two dimensional function $f : \mathbb{Z}^2 \to \mathbb{Z}$. Gray-scale image is then described by one function of intensities, whereas colour image needs three functions for the red-scale, green-scale and blue-scale to create the desired colour. Intensity histogram $H : \mathbb{Z} \to \mathbb{Z}$ can be derived from the values of pixels as:

$$H(i = m) = N_m,$$

where N_m is the count of pixels with intensity m and i is the range of all possible intensities. Intensity histogram carries the information about the intensity spectrum, showing number of pixels of a certain intensity.

In this chapter different algorithms of multiple analysis tasks and different approaches will be discussed. Some algorithms will be examined in more detail to illustrate the variety of approaches and options for data analysis. Approaches vary in multiple ways, from simple image processing tasks, convolutional neural networks to approaches like stereological methods.

3.1 Registration

The imaged object in three dimensions is transformed by the microscope to a z-stack, which is a series of two dimensional images, where the third dimension is saved in the continuity of the stack. The best quality in three dimensions can be achieved by multiview imaging. This method, however, brings a challenge of stitching different views into one resulting z-stack. This problem is known as multi-view image registration and is used in 3D image reconstruction, generating large field of view and satellite imaging [33]. Multiple methods and algorithms have been proposed, such as [34, 35, 33] not only for microscopy images. This work will cover one of them.

Method used in [34] uses fluorescent beads in the image acquisition for best results of the registration. However, using the beads is not always possible, as the beads must be submerged in a solid medium to stop them from changing their position. These beads are then used as features in the algorithm, if beads are not used other distinct objects in the images must be used, for example nuclei. The algorithm calculates mutual distances amongst the features and defines each feature by their neighbouring features. This is a translation and rotation invariant local geometric descriptor, which is preserved for each feature across different views. They transform their space into an orthogonal coordinate system, in which each feature and its 3 closest neighbours can be described by a vector of six values. In every view in the six-dimensional space, specific constellation of four features would be described by descriptors whose Euclidean distance amongst each other would be very small, even zero. Thus, they searched for closest feature descriptors and false positives were discarded by random sample consensus and robust regression filter. After registration, fusion of all the views into one z-stack needs to be calculated, this operation is usually joined with deconvolution.

3.2 Deconvolution

Deconvolution is an operation to increase quality and the resolution of a microscopy image; and to reconstruct the original object. As the image is acquired by convolution of the object according to the point spread function, which has been defined in Chapter 1.3, this leads to reducing the quality. To deconvolve an image, point spread function needs to be known. If true PSF is known, as a function of the diffraction of a point light source in the microscope, then deconvolution of the image would be just a mathematical operation. However, this point spread function does not carry information about other possible degradations of the quality, like noise or aberrations. An estimate of the whole degradation function can be theoretically and experimentally derived, either iteratively approximated or estimated by calibrating with imaging beads.

Deconvolution of functions as defined in mathematics is simply done in the frequency domain. If we have a convolution $f * g$ of two functions f and g, then Fourier transform of the convolution is defined as follows:

$$\mathcal{F}(f * g) = \mathcal{F}(f) \cdot \mathcal{F}(g).$$

Thus, deconvolution is simply:

$$\mathcal{F}(f) = \frac{\mathcal{F}(f*g)}{\mathcal{F}(g)}.$$

Function f is derived by applying inverse Fourier transform, which is the object O that is the desired reconstruction from the acquired image I divided by PSF in the frequency domain. However, in image deconvolution the process is not as simple due to the addition of noise.

PSF of the microscope can be derived experimentally. The microscope is used for imaging fluorescent beads with an ideal diameter below 50 nm (usually $100 - 200$ nm) first. During the experiment microscope should be used under the same conditions as for PSF calibration. From these images the point spread function is calculated. After acquiring the point spread function, the deconvolution is done iteratively. A possible reconstructed object image is estimated, convolved with the PSF and compared to the observed image. Their difference is calculated and the process is repeated with a different estimation, which is recalculated based on the difference. Iterations are stopped, when one of two constrains are met, either maximum number of iterations or critical value of the difference, quality criterion. After acquiring the PSF, only the noise needs to be estimated to find the image of the reconstructed object.

As a first estimation of the reconstructed image, Wiener filter is employed. Wiener filtering proposes minimizing the function, which expresses the difference between observed image and the convolved estimation, as a least square loss: $||I - \hat{O} * PSF||^2 - ||n||^2$, where n expresses the noise and $\hat{O}$ is the estimation of object [16]. Inverse filtering is filtering on the principle of the least square function, however noise is not included.

Multiple algorithms may be used for the iterative process: constrained iterative algorithms and statistical algorithms. Further statistical algorithm employing maximum likelihood estimation (MLE) is described, as this one is widely used, for example by SVI Huygens. Statistical approaches are based on the Bayesian theorem of conditional probability, where following is true: $P(O|I) = \frac{P(I|O)\times P(O)}{P(I)}$.

The object O is represented by its prior probability density $P(O)$, image I by $P(I)$, the conditional probability $P(I|O)$ to model the degraded object I given object O and posterior probability $P(O|I)$ of object O given the observed degraded image I. The MLE algorithm finds the reconstructed object $\hat{O}$, which maximizes the posterior probability. The conditional probability $P(I|O)$ is estimated from a Poisson distribution:

$$P_{Poisson}(x|\mu) = \frac{\mu^x e^{-\mu}}{x!},$$

where the result gives the probability that x is the observed noisy datum, when μ is the noise-free average value. Every pixel of the image is assumed to be statistically independent, the probability is the product of probabilities of individual pixels as follows:

$$P_{Poisson}(I|O) = \prod_{i=0}^{W+H} P_{Poisson}(I_m|O_m),$$

where I_m and O_m are individual pixels. To simplify the calculation negative logarithm of the probability is minimized in further steps, this function is called log negative likelihood. The minimum is found by setting the derivative to zero. From the minimum, the update for the estimated object in k-th iteration is found as:

$$\hat{O}_m^{k+1} = K\hat{O}_m^k \sum_l (PSF_{m-l} \frac{i_l}{\sum_n PSF_{l-n}\hat{O}_n^k})^p,$$

where p is a constant and K is a constant to ensure energy conservation. Initialization of $\hat{O}_m^0 = I_m$.

Blind deconvolution is used for experiments, where the PSF is unknown, as it has not been estimated from the beads. In each iteration the object and PSF are estimated. The algorithm uses MLE as before, however the object estimate $\hat{O}$ is updated each iteration as MLE estimate and PSF estimate $\hat{PSF}$ is updated accordingly. The initialization of the object estimate $\hat{O} = I$ is assigned to the observed image and $\hat{PSF}$ is initialized by a theoretical PSF of the microscope [16].

In deconvolution proclaiming SNR of the observed image is used in the algorithms. However, the estimate may change the result, as SNR too low may lead to too smooth image, as small objects have been mistaken for noise and removed. If declared SNR is too high artefacts, in the form of tiny objects or ring artefacts, can arise or noise is enhanced.

Other deconvolution algorithms are available, using different than statistical approaches like in [36] or even improving deconvolution for novel microscopy technologies, for example for LSFM in [37], which is available in MATLAB. MLE approach is widely used, as it is robust to noise and simple. However, the convergence of the reconstructed object is slow and the computation each iteration is more demanding.

3.3 Segmentation

Segmentation is a very important task, when the desired outcome focuses on certain objects in the images. Result of segmentation is a binary mask of the image that carries the information, whether a specific pixel belongs to an object or not. Segmentation and the final binary image can be described by a function $b : \mathbb{Z}^2 \to \mathbb{Z}$:

$$b(x,y) = \begin{cases} 0 & \text{if f(x, y) does not belong to an object} \\ 1 & \text{else} \end{cases},$$

here $x \in 0, ..., W$ and $y \in 0, ..., H$ are possible positions in the image with resolution $W \times H$.

Segmentation is a very complex task, main goal is typically segmentation of particular cells or certain organelles. Segmentation of cells has shown to be very difficult to be generalized, depending greatly on the imaging method and the imaged tissue or cell type [38].

Approaches to this task vary gravely, depending on the level of expertise of the user. The easiest approach used in many bioimage software is simple threshold method using tools like watershed. Segmentation can be done by stereological methods as well, which is implemented in a special software. Next approach belongs to a simple image processing and requires some programming skill, as this is not usually used in the bioimage programmes. The last approach is application of neural networks, which usually requires some understanding of computer vision and programming, as the inclusion of neural networks is new in many software and sometimes lacks in the user-friendliness.

For the best results normalization of the image intensity should be always applied, as the full spectrum of intensity will be better utilized. Normalization is defined as:

$$f'(x,y) = \frac{M \cdot f(x,y)}{\max f(x,y)},$$

where M is the largest possible value for the intensity (usually taken 255), $x \in 0, ..., W$ and $y \in 0, ..., H$ are possible positions in the image with resolution $W \times H$, $f(x,y)$ is the original image function and $f'(x,y)$ is the function after normalization.

3.3.1 Threshold

Detecting objects in an image is a task of differentiating, which pixels belong to the object. In some cases it can be easily identified if the intensity of the object is different from the intensity of the background and other objects. To segment desired objects only the threshold intensity needs to be found, usually lower bound of the intensity is sufficient, however upper threshold for the intensity can be found similarly. This can be done automatically or manually. Segmentation using threshold intensity t is a binary function $b : \mathbb{Z}^2 \to \mathbb{Z}$ defined as:

$$b(x,y) = \begin{cases} 0 & \text{if f(x, y)} \leq \text{t} \\ 1 & \text{if f(x,y)} > \text{t} \end{cases},$$

where the variables are defined as above.

By programming, the simplest approach is to iteratively try all the values of possible intensity and choose the best result by confirming, whether the mask extracts the objects correctly. Another approach is extracting the threshold from the intensity histogram, where ideally a valley is seen between two peaks of intensities, where the middle of the valley can be deducted to be approximation to the best value. Automatic and unsupervised solution used in image processing and computer vision is Otsu's method [39]. This technique has been proposed

to overcome difficulties such as, flat and wide valley or insufficiently defined two peaks with hardly identifiable valley [39]. Two classes are created C_0 for the background and C_1 for the extracted objects. Then the algorithm minimises the sum of the variances of pixels in those two classes, which means most similar intensity of pixels are grouped into the same class. In the algorithm this optimization is found as maximizing inter-class variance (minimizing intra-class variance), which is calculated by iteratively changing the threshold intensity.

Life science imaging software often offer segmentation modules, which can be applied by moving a threshold slider looking for the best differentiation of objects. Sometimes this functionality is accompanied by a watershed tool. Watershed tool offers gradual segmentation, where from a desired pixel of a certain intensity the mask spreads over pixels with the same intensity and gradually higher as the threshold is changed. More of these tools may be used, like brush or lasso, which define the area of segmentation further and others. Some software offer more automated version, where user needs to define properties, like expected size of the object and the width of the boundary.

Biggest problem for these solutions may be inconsistent intensity throughout the picture and grouped objects, where identifying border may be difficult [40]. These methods, however, may be effective for the whole volume of the objects dyed fluorescently, for example DAPI for nucleus segmentation.

3.3.2 Image processing

There are many ways, in which image can be adjusted to better the quality of segmentation and to find the threshold more effectively and with better accuracy. There has been made attempts to make segmentation algorithms more generalized having good results for multiple types of cell and imaging methods.

Method proposed in [38] has developed a framework for a more inclusive cell segmentation. Firstly, they employed edge detection using Sobel operator to obtain a gradient image, which emphasises edges. Afterwards, original and gradient image are both normalized to achieve uniformly spread intensity over the grey-scale. Both images are afterwards filtered in the frequency domain, which is achieved by transforming the normalized histogram distribution $H(i)$ with the Discrete Fourier Transform (DFT) and the higher frequencies are eliminated to adjust the histogram to be smoother. To obtain histogram inverse DFT must be applied. Afterwards, peaks and valleys of the histogram are found and the threshold is chosen depending on the properties of valley and peaks.

3.3.3 Stereology

Stereology is a field, which deducts three-dimensional information, such as volume (even volume of a specific region, like cartilage repair tissue [41]), size, shape or cell count, from two-dimensional images creating a stack. Stereological methods employ various sampling techniques and tools to obtain quantitative data [42]. Stereology employs probes (planes, lines, points or their combination) to virtually section the images and obtain specific information about the interaction of probes and features. For example, to calculate volume v of an imaged object, virtually cut the object by a plane, calculate intersection area a of the object and

the plane, and from knowledge of the height h of the object (calculated perpendicular to the plane) an estimation of volume can be obtained as $v = a \cdot h$. This is one estimation of the volume, and if the procedure is repeated multiple times (ideally infinite times) an unbiased estimation of the volume is derived as a mean of all the estimations. This method is undermining the importance of the shape on the volume and may create bad estimations, thus more complex sampling and methods should be employed [43]. Instead of planes, lines may be used, to count intersections of the probe (line) with the desired feature (cell or the edge of the object to estimate surface). Sampling can be systematic or random, randomness is needed for unbiased estimations, however systematic sampling gives more information about statistical variance and efficiency. Usually, the first probe is chosen at random and subsequently some systematic sampling is employed, for example parallel planes are projected equidistantly, or lines regularly spaced [43].

Cell counting using stereological methods may be done by using multiple types of probes, such as optical fractionator or dissector. Dissector is used mainly for thin samples or monolayer samples (in Petri dish). Dissector is modified square with two halves. Cells touching one half are counted, cells touching the other are not counted. From the sampled area cell density is calculated and cell count is predicted. Optical fractionator is used for thick samples, where planes are used as probes. If plane intersects top of a cell, the cell is counted. Counting only the top prevents multiple counts of one cell. Cell density in a volume is used again for the cell count estimate of the whole sample.

3.3.4 Neural networks

Theory in this section is taken from [44], which is a detailed source for neural networks and deep learning. One of the popular machine learning models are neural networks, other machine learning models may be logistic regression, support vector machines or Bayesian classifier, which has also been used for cell segmentation [45]. Machine learning solves problem of predicting an outcome y from data example x based on iteratively learned parameters θ, such that $y = f(x; \theta)$. One kind of machine learning is supervised learning, where for each example from the training data a target label is available. The example x is usually defined by numerous features represented as a vector of real numbers. For example, an airplane can be represented by its speed, flight range and number of seats, which are stored as a vector of three real numbers. A black-and-white image of $n \times n$ is represented as vector with n^2 numbers, each representing intensity at a certain pixel. Predictions assigned to each example may be categorical or continuous. Categories are for example different types of airplanes, object appearing in an image or whether specific pixel in the image belongs to an object. Continuous values are represented by real numbers, for example capacity of an airplane tank. Based on the input feature vector and target labels the network learns the parameters θ.

Neural networks are comprised of neurons with nonlinear activation functions, for example $\max(0, x)$. Neurons are grouped into hidden layers and each layer is defined as $h = g(Wx)$, where g is the activation function, W their parameters, which are iteratively changed and x input data. Altogether all hidden layers make up the prediction function.

Prediction function $f(x;\theta) : X \to Y$, a mapping from training data X to the predictions Y, is trying to minimize the prediction error function $\mathcal{L}$ called loss. Loss function describes how close the predictions are to the target labels and few possible functions may be used, such as mean square error, mean absolute error or negative log likelihood (cross entropy loss), which is used in [46] and is defined as:

$$\mathcal{L} = -(y \log(p) + (1 - y) \log(1 - p)),$$

where p is the probability of default class (the background), log is the natural logarithm. This formulae applies to prediction problems with two possible classes (the background or the object).

Improving the prediction function is done iteratively by computing gradient of the loss function with respect to the parameters θ: $\Delta_\theta \mathcal{L}(X, Y; \theta)$ and propagating the gradient through each neuron called gradient descent. Networks implementing stochastic gradient descent do not calculate the gradient for all training examples, however for a fixed batch of the examples as their average.

Convolutional neural networks (CNNs) are used for data with grid-like topology, for example 2D images. CNNs use convolution (convolution is a mapping as defined above) for image analysis, in this case a mapping between two image spaces. Thus, it can be considered as a sliding window moving over the image. The result is a new image calculated from the original image and the values in the convolution window called kernel. Kernel is represented as a square matrix, usually of dimensions 3×3, 5×5, etc. Convolution of an image and the creation of new image is portrayed in Figure 3.1. It is conventional to apply activation nonlinear function on the resulted image.

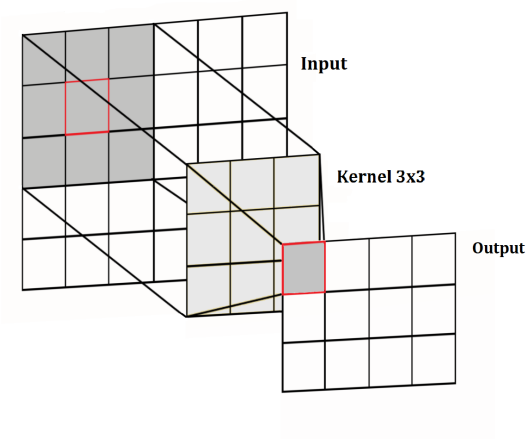

Figure 3.1: Convolution of input image 5×6 with a kernel 3×3 with valid padding resulting in output image of 3×4.

Convolution layer can have multiple modes, valid or same padding and optional stride can be set. Stride is the step size over the image with the sliding window, for stride one the sliding window moves by one pixel between operations, stride two moves by two pixel thus decreasing the pixel size of the created image. Convolution mode, after which the resolution is lost for the border pixels, is called valid padding. If resolution should be preserved, same padding should be applied, which adds new pixels to the edge of the image with arbitrary value,

usually 0. Pooling layers are used to downsample data, which means to decrease their resolution $W \times H$. Upsampling is increasing the resolution. Pooling is done with a kernel, usually 2×2 and stride 2. From the original image in the window of 2×2 is taken specific value as a new pixel, thus from 4 pixels is created 1, thus decreasing the resolution. Values are taken by criterion, for example maximum value (max-pooling), or average value.

U-Net

In [46] the architecture of the network used is called u-net, as it resembles u-shape. The architecture is shown in Figure 3.2. The desired prediction of the model is a class label for every pixel, in this case whether the pixel belongs to the segmented object or not, creating a binary mask.

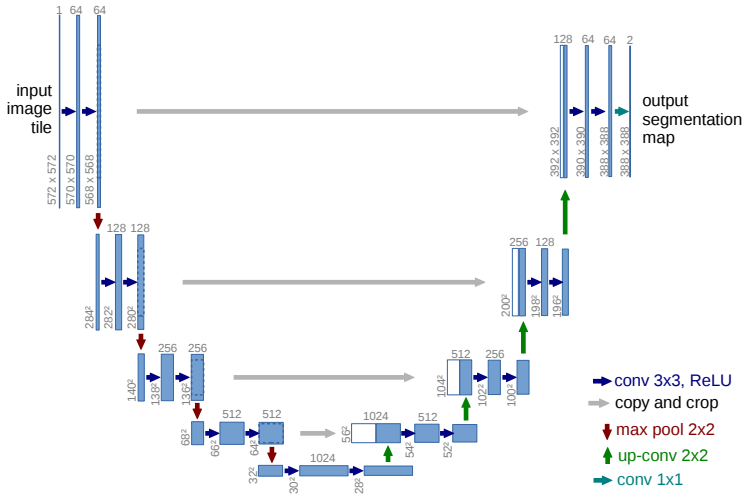

Figure 3.2: The u-net architecture employed in [46] for segmentation. Image taken from [46].

The u-net architecture builds upon fully connected network. Layers use convolution kernels and are derived into few parts, contracting path to downsample the data and expansive path to upsample data. Altogether 23 layers are used. As can be seen in Figure 3.2 in every level is a convolution with 3×3 kernel with a function rectified linear unit (ReLU), $\max(0, x)$. To downsample max-pooling layer with convolution kernel 2×2 with stride 2 is used. To upsample is used up-convolution with kernel 2×2 and concatenation with copy of the cropped feature vector from the same level of contracting path. Number of feature channels is changed accordingly: doubles when data are downsampled, halves when upsampled. The output layer takes the feature vector and outputs the predicted class. As all the convolution layers used valid padding the feature vector got cropped in the result and output layer.

3.4 Quantitative analysis

For quantitative analysis multiple variables may be observed. Segmented cells may be counted or tracked, volume of segmented material may be measured in ratio to the volume of the sample. Cell counting in 3D is a difficult task as one

cell is present in multiple images in the stack. The simplest algorithm imaginable is to connect segmented components, when they are connected (neighbouring pixels) in the z-direction . This algorithm however undermines grouping of touching objects and is unable to separate them. In [40], multiple approaches to 3D cell segmentation have been reviewed with the conclusion of the superiority of stereological cell counting over the automated algorithms.

Tracking is important for live cell imaging, distance passed and speed can be derived from tracking cells. Tracking is done easiest for cell moving in the direction of one slice, not in the z-direction.

3.5 Visualization

Visualization of the images is very important part of the experiment, as it needs to encompass the results and the importance of the experiment. As there are numerous technologies to image samples, there are even more ways to visualize them. For visualization the pictures with the best quality are taken, enhanced by denoising or deconvolution, however there is a line between enhanced images and image with added artefacts as a result of those procedures. For two dimensional images visualization tends not to be difficult, as only the final image needs to be selected and the desired outcome needs to be shown properly, whether via showing segmented objects or via showing the enhanced quality.

Three dimensional stacks of images impose a bigger challenge. There are multiple modes of displaying the whole volume of the image, and multiple projections are used, for example maximum-intensity projection (MIP). Volume rendering tends to be viable when showing surfaces of objects or segmented objects in the whole volume, usually via MIP or by volume rendering the binary mask derived as a result of segmentation or surface reconstruction. If the whole volume is not needed to be shown, orthogonal and even user-defined slices may be shown as two dimensional images from the z-stack. In these images either surface rendering (its border) or segmented objects can be visualized nicely. Moving through the slices can be shown by animation.

With LSFM time lapses of z-stacks of images, there is a fourth dimension, which cannot be easily shown in one image, and either series of images may be shown, the usage of animation is better suited for this task.

3.6 Workflow

Preparation of imaging data from LSFM and extraction of valuable results is completed in few steps, the most usual steps are as follows:

- Multi-view registration
- Multi-view fusion and deconvolution
- Visualization
- Analysis - quantification of cells, tracking of cells
- Result demonstration

4. Solutions Available

4.1 Overview of available software

There is a wide selection of software available on the market for bioimage analysis, ranging from commercial products, software for the microscopes to open-source free software. Commercial products tend to be directed for laboratories and imaging facilities, whereas open-source free software can be used by novice analysts or enthusiasts, as well as professionals.

4.1.1 FIJI

FIJI is an open-source free image processing distribution of ImageJ, developed for further, more complex bioimage analysis. As it is open-source, algorithms used, their documentation and tutorials are readily available. It is customizable by adding custom plug-ins and other components. However, due to its graphical user interface and easy navigation it is easy to use for beginners and for algorithm developers alike [47]. FIJI offers both simpler image processing, like changing colour intensity, cropping and such, and complex analysis. It offers MultiView Fusion and Deconvolution for Light-sheet microscopy images and segmentation by thresholding and other algorithms. Developers of FIJI are developing neural network options as well for numerous purposes, like for denoising and segmentation. It was build as a community for enthusiasts and image analysts with a forum as a platform for advice and help.

4.1.2 Amira

Amira is a software from Thermo Fischer Scientific for visualization, manipulation and analysis of life science images. It offers multiple algorithms suitable for denoising, filtering, alignment of images and segmentation. Numerous visualization techniques may be employed, it offers both 2D and 3D visualization options and tool to create animations. 3D visualization can be by rendering 3D volume in a MIP or other settings or by moving through the slices. Some of the algorithms, for denoising and filtering, have been developed to run parallelly or on graphics processing unit (GPU). It offers integration of Matlab and can be operated by TCL scripting language or Python.

4.1.3 Imaris

Imaris is a software from Oxford Instruments. It offers analysis of 2D, 3D and 4D data, as well as their visualization in multiple possible ways - animation, volume rendering or slicer. It offers surface of objects reconstruction, segmentation, simple measurements, colocalization, spots detection and filament tracking. The whole workflow is done in a wizard helping to get through the process and offers visual fine-tuning parameters, which can be adjusted and user right away sees difference in the result. It is suitable for fluorescent images, especially z-stacks.

It offers integration of Matlab and Python, by using module XTensions adding plug-ins is possible [47].

4.1.4 Arivis

Arivis Vision4D is a software suitable for working with 2D, 3D and 4D images. It is optimized for big data, as it is opened in a proprietary file format [47]. It offers main tools, for alignment, cell segmentation, tracking, visualization, annotation and is advised for stitching multiple datasets of the whole imaged object. It offers integration of Matlab and Python, where user can write pipelines of operations.

4.1.5 SVI Huygens

SVI Huygens is a software for image deconvolution. It offers deconvolution of datasets acquired on numerous types of microscopes, blind deconvolution, estimation of PSF from imaging beads and offers a tool Fusion and Deconvolution for LSFM. It also offers correction tools for chromatic aberration, crosstalk and drift. Datasets can be visualized in Huygens, results of the deconvolution and corrections can be easily compared in a side-by-side view, as well as observation of their intensity histograms.

4.1.6 ZEN

ZEN is a software from Zeiss. It is useful for acquiring images from the microscopes, it allows visualization and detection of desired objects in the sample, which can then be imaged. It offers tools for visualization of stacks, processing tasks like intensity adjustment, multichannel view, deconvolution and fusion of LSFM data.

4.2 Comparing software

4.2.1 Comparing deconvolution in SVI Huygens

I used SVI Huygens to deconvolve one dataset with multiple settings to observe the results, compare the importance of choosing right parameters and illustrate the importance of quality image acquisition. The dataset was acquired as 283 slices in dual-view mode and by illumination with two lasers on Lighsheet Z.1. I have tried deconvolution on each view, from left and right, on both views at once using Fusion and Deconvolution tool; and on already fused dataset (fused by ZEN). I have changed one parameter, signal-to-noise ratio to acquire the best improvement of the quality. Used SNR was 60, 30, 15 and 5. As opposed to the first estimate, which was 20-30, the best results were acquired by setting $SNR = 5$.

In Figure 4.1 one slice (number 49/283) from the z-stacks can be seen, magnified. Images shown are taken from datasets: before deconvolution and after deconvolution with two settings of SNR 5 and 30. Only one view is shown. In the image deconvolved with $SNR = 30$ enhanced noise can be seen, whereas

image with $SNR = 5$ shows reduced noise, reduced background intensity and increased contrast.

In Figure 4.2 the slice 49 is shown again. Datasets used are without deconvolution, showing one view and fused dataset. Slight degradation, in the form of more prevalent background, of the fused dataset can be seen, as the multi-view imaging has produced only one view with high quality and the other view is of very low quality with lot of noise.

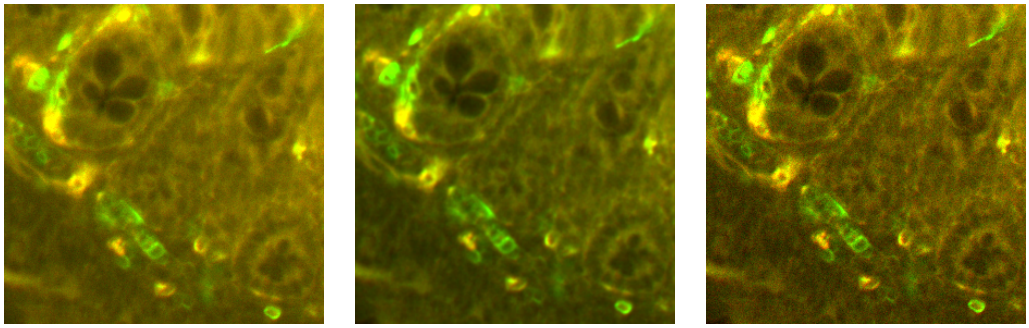

a) Original b) SNR = 5 c) SNR = 30

Figure 4.1: Images deconvolved in SVI Huygens.

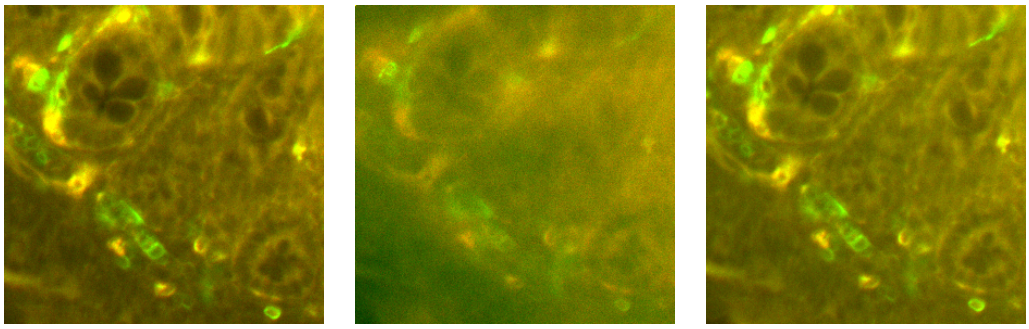

a) Right view b) Left view c) Fused

Figure 4.2: Images acquired by Lightsheet Z.1 by multi-view imaging, from each view and fused by ZEN.

4.2.2 Comparing computational capabilities

As the microscopy technologies evolve, the analysis tools evolve as well and are accustomed to the new conditions. One of the main demands to analyse LSFM data is the ability of the software to handle large data and the optimization to use as much of the computational power as possible. Single dataset from Lightsheet Z.1 can have size in the order of tens of gigabytes or even hundreds of gigabytes.

To compare how Imaris, FIJI and Amira handle data, dataset of size 7.77 GB has been opened and simple processing and visualization has been conducted to observe their computational options. Machine used for these observation has parameters in Table 4.1. Different algorithms have been observed to obtain information, whether they are parallelized; and whether they run on CPU

or on GPU. Using GPU allows for much higher analysis and processing speed. Amount of storage, which is needed to analyse the data has been noted as well, and whether the file can be stored in RAM for faster acquisition and processing.

Task such as alignment, filtering and rendering have been observed. Alignment is used, when some images are slightly shifted, which may be result of drift during acquisition. Alignment is not as needed for LSFM images compared to images from SEM for example. Filters are used for denoising or blurring (which leads to less noise). Many filters may be used, common are Gaussian filter or median filter.

Intel Xeon CPU	3.70GHz, 8 cores, 16 threads
NVIDIA Quadro RTX 5000 GPU	16GB VRAM
RAM	128GB

Table 4.1: Technical parameters of used machine.

Amira gives several options of opening the dataset: whether the file should be opened from RAM, disk or converted to a proprietary file format, which should help with management of large datasets with lower storage available. To open file formats, which belong to the BioFormats, for example .czi a proprietary file format from Zeiss microscopes. After opening the dataset in RAM, Amira creates new dataset after every operation, thus the amount of storage needed is high and it is advisable to remove unneeded datasets from Amira. For alignment of images Amira used 50% of CPU and increased memory, when using function AutoAlign. However, only 8% of CPU, when using function Align. Thus, user should test, which functions are parallelized, as their purpose and results are the same. Alignment algorithms have not been written for use on GPU. To render 3D volume, Amira used around 95% of CPU.

Imaris can load only files in proprietary file format, and the conversion is done before opening the file, converted file is the size of the original. The file is opened in RAM memory, the amount of memory used is the size of the file. After each operation, the memory usage increases, usually adds the size of the dataset as new version is created. When rendering, Imaris uses GPU, for example when the dataset is moved around. Tested filters were Gaussian and median. Gaussian filter used on average 85% of CPU and the stored data on RAM increased by original size. Median filter used only on average 13% of CPU and the size in RAM also increased by that amount. Filtering algorithms have not been written for use on GPU. While aligning images on average 95% of CPU was used and the size increased by the size of original dataset.

Files are loaded in multiple formats, supports BioFormats. Files are loaded and stored in RAM during the analysis. Dataset in the form of z-stack is automatically opened as a series of images, each view and channel separate. Size used in RAM after opening the dataset is slightly higher than the size of dataset at around $10GB$. Gaussian filter uses 83% od CPU, none GPU and the size on RAM increases by the size of dataset. Median filter uses 97% of CPU, none GPU and the size increases the same. To enable processing on GPU, plugin CLIJ has been developed. Amongst GPU-accelerated algorithms supported are morphological filters, spatial transforms, image warping, local and global thresholding, minima/maxima detection, logical operations on binary images, 3D-to-2D

projections, and methods of descriptive statistics for quantitative measurements [48]. However, it is recommended to use CLIJ for users with entry-level programming skills. Using CLIJ does speed up the processing and analysis as is shown compared to using CPU [48].

Conclusion

Bioimage analysis is a key part of microscopy and studies dependent on images acquired by microscopes. In this thesis, I have summarized different tasks in the analysis, different problems in microscopy and different technologies behind. Bioimage analysis is an important part of the experiment offering not only visualization of results, but also quantitative data as well.

The microscopy technologies are diverse and the field is still growing. Since the topic and options are very broad, the tasks in bioimage analysis and approaches to solving the tasks are various. This has been shown by multiple approaches to all of the tasks covered in this thesis.

I have described concept of microscopes, both light and electron, as the usage of electron microscopy in life science is on the rise. I have focused in more depth on fluorescence microscopy, engaging in describing the phenomenon of fluorescence and its opportunity of studying tissues and histological samples. Furthermore, I have covered the light-sheet fluorescence microscopy, which offers new possibilities in developmental studies, however brings new challenges in the form of handling large data.

In the image analysis part, I have summarized multiple tasks in the analysis and some already employed algorithms. As seen in the thesis, many different approaches exist and are used, from neural networks, which are developed by computer vision engineers to simple image processing, which can be found in multiple available software. Software available on the market has also been covered. Multiple different options with different tools and approaches have been shown. I have also compared different computational and storage requirements for using different software.

As microscopy is important part of many experiments and inseparable part of life science, the demand for bioimage analysis is rising. New technologies are bringing amounts of data that manually cannot be analysed and thus analysts with the knowledge of multiple solutions, whether programmatically or by employing existing software, are needed. Either using neural networks or stereology, segmentation is valuable and necessary task, to count or track cells, often observe their division or apoptosis.

List of Abbreviations

SNR	Signal-to-noise ratio
LSFM	Light sheet fluorescence microscope
SPIM	Selective-plane illumination microscope
GFP	Green fluorescent protein
CCD	Charge-coupled device
sCMOS	scientific Complementary metal–oxide–semiconductor
PSF	Point spread function
MLE	Maximum likelihood estimation
MIP	Maximum intensity projection
DFT	Discrete Fourier transform
CNN	Convolution neural network
GPU	Graphics processing unit
CPU	Central processing unit

Bibliography

[1] Thomas A. Klar, Egbert Engel, and Stefan W. Hell. Breaking Abbe's diffraction resolution limit in fluorescence microscopy with stimulated emission depletion beams of various shapes. *Phys. Rev. E*, 64:066613, Nov 2001.

[2] Emmanuel Reynaud, Jan Peychl, Jan Huisken, and Pavel Tomancak. Guide to light-sheet microscopy for adventurous biologists. *Nature methods*, 12:30–4, 12 2014.

[3] Petr Malý. *Optika*. Karolinum, 2013.

[4] Greenfield Sluder and Joshua J. Nordberg. Chapter 1 - microscope basics. In Greenfield Sluder and David E. Wolf, editors, *Digital Microscopy*, volume 114 of *Methods in Cell Biology*, pages 1 – 10. Academic Press, 2013.

[5] R. Egerton. *Physical Principles of Electron Microscopy: An Introduction to TEM, SEM, and AEM*. Springer ebook collection / Chemistry and Materials Science 2005-2008. Springer US, 2011.

[6] Joseph R. Lakowicz. *Principles of fluorescence spectroscopy*. Kluwer Academic / Plenum Publishers, Second edition, 1999.

[7] Kurt Thorn. A quick guide to light microscopy in cell biology. *Molecular Biology of the Cell*, 27:219–222, 01 2016.

[8] A. B. Cubitt, R. Heim, S.R. Adams, A.E. Boyd, L.A. Gross, and R.Y. Tsien. Understanding, improving and using green fluorescent proteins. *Trends in biochemical sciences*, 20(11):448—455, November 1995.

[9] Maureen R. Hanson and Rainer H. Köhler. GFP imaging: methodology and application to investigate cellular compartmentation in plants. *Journal of Experimental Botany*, 52(356):529–539, 04 2001.

[10] Richard N. Day and Michael W. Davidson. The fluorescent protein palette: tools for cellular imaging. *Chemical Society Reviews*, 38:2887–2921, 2009.

[11] Karl Jansen, Bengt Norden, and Mikael Kubista. Sequence dependence of 4',6-diamidino-2-phenylindole (DAPI)-DNA interactions. *Journal of the American Chemical Society*, 115(23):10527–10530, 1993.

[12] Jan Kapuscinski. DAPI: a DNA-Specific Fluorescent Probe. *Biotechnic & Histochemistry*, 70(5):220–233, 1995.

[13] Karen G. Porter and Yvette S. Feig. The use of DAPI for identifying and counting aquatic microflora 1. *Limnology and oceanography*, 25(5):943–948, 1980.

[14] Douglas B. Murphy and Michael W. Davidson. *Fundamentals of light microscopy and electronic imaging*. Wiley-Blackwell, 2013.

[15] Peter G. Bush, David L. Wokosin, and Andrew C. Hall. Two-versus one photon excitation laser scanning microscopy : Critical importance of excitation wavelength. *Frontiers in Bioscience*, 12:2646, 01 2007.

[16] Jean-Baptiste Sibarita. Deconvolution Microscopy. *Advances in biochemical engineering/biotechnology*, 95:201–43, 02 2005.

[17] Paul C. Goodwin. Chapter 15 - evaluating optical aberrations using fluorescent microspheres: Methods, analysis, and corrective actions. In Greenfield Sluder and David E. Wolf, editors, *Digital Microscopy*, volume 114 of *Methods in Cell Biology*, pages 369 – 385. Academic Press, 2013.

[18] Tytus Bernas, Bartlomiej P. Rajwa, Elikplimki K. Asem, and Joseph Paul Robinson. Loss of image quality in photobleaching during microscopic imaging of fluorescent probes bound to chromatin. *Journal of Biomedical Optics*, 10(6):1 – 9, 2005.

[19] George Patterson and David Piston. Photobleaching in Two-Photon Excitation Microscopy. *Biophysical journal*, 78:2159–62, 04 2000.

[20] Herbert Schneckenburger, Petra Weber, Michael Wagner, Sarah Bruns, Verena Richter, Thomas Bruns, W.S.L. STRAUSS, and Rainer Wittig. Light exposure and cell viability in fluorescence microscopy. *Journal of microscopy*, 245:311–8, 11 2011.

[21] Jérémy Surre, Claude Saint-Ruf, Valérie Collin, Sylvain Orenga, Mahendrasingh Ramjeet, and Ivan Matic. Strong increase in the autofluorescence of cells signals struggle for survival. *Scientific Reports*, 8, 12 2018.

[22] Olaf Selchow and Jan Huisken. Light sheet fluorescence microscopy and revolutionary 3D analyses of live specimens. 2013.

[23] Jaroslav Icha, Christopher Schmied, Jaydeep Sidhaye, Pavel Tomancak, Stephan Preibisch, and Caren Norden. Using Light Sheet Fluorescence Microscopy to Image Zebrafish Eye Development. *Journal of Visualized Experiments*, 2016, 04 2016.

[24] Hans-Ulrich Dodt, Ulrich Leischner, Anja Schierloh, Nina Jährling, Christoph Mauch, Katrin Deininger, Jan Deussing, Matthias Eder, Walter Zieglgänsberger, and Klaus Becker. Ultramicroscopy: Three-dimensional visualization of neuronal networks in the whole mouse brain. *Nature methods*, 4:331–6, 05 2007.

[25] UltraMicroscope II: Fast 3D Imaging of Entire Biological Systems. `https://www.lavisionbiotec.com/products/UltraMicroscope.html`, [Online] Last accessed on 3.01.2020.

[26] Selective Plane Illumination Microscopy by ASI. `http://www.asiimaging.com/products/light-sheet-microscopy/`, [Online] Last accessed on 29.12.2019.

[27] Peter G. Pitrone, Johannes Schindelin, Luke Stuyvenberg, Stephan Preibisch, Michael Weber, Kevin W. Eliceiri, Jan Huisken, and Pavel Tomancak. OpenSPIM: an open-access light-sheet microscopy platform. *Nature Methods*, 10(7):598–599, Jun 2013.

[28] Emilio J. Gualda, Tiago Vale, Pedro Almada, José A. Feijó, Gabriel G. Martins, and Nuno Moreno. OpenSpinMicroscopy: an open-source integrated microscopy platform. *Nature Methods*, 10(7):599–600, July 2013.

[29] Corinne Lorenzo, Céline Frongia, Raphael Jorand, Jérôme Fehrenbach, Pierre Weiss, Amina Maandhui, Guillaume Gay, Bernard Ducommun, and Valérie Lobjois. Live cell division dynamics monitoring in 3D large spheroid tumor models using light sheet microscopy. *Cell division*, 6:22, 12 2011.

[30] Lee Hwee-Kuan, Weimiao Yu, John Lim, and Sohail Ahmed. Light Sheet Fluorescence Microscopy (LSFM); Past, Present and Future. *Analyst*, 139, 07 2014.

[31] P.M. Flood, R. Kelly, L. Gutiérrez-Heredia, and E.G. Reynaud. Sample Preparation. 2013.

[32] Microscopy Nyquist rate and PSF calculator. `https://svi.nl/NyquistCalculator`, [Online] Last accessed on 5.01.2020.

[33] Mital S. Patel, N.M. Patel, and Mehfuza S. Holia. Feature based multi-view image registration using SURF. pages 213–218, Sep 2015.

[34] Stephan Preibisch, Stephan Saalfeld, Johannes Schindelin, and Pavel Tomancak. Software for bead-based registration of selective plane illumination microscopy data. *Nature methods*, 7:418–9, 06 2010.

[35] KaiXing Wu, Juan Hao, and ChunHua Wang. The Research Based on Multi-view Image Registration. *Communications in Computer and Information Science*, 227, 08 2011.

[36] Ming Wang and Jin Li Yao. The Research and Development of Restrained Iteration Deconvolution Algorithm in Three-Dimensional Microscope Image Restoration. pages 1487–1490, Dec 2009.

[37] Klaus Becker, S. Saghafi, Marko Pende, Inna Sabdyusheva, Christian Hahn, Massih Foroughipour, Nina Jährling, and Hans-Ulrich Dodt. Deconvolution of light sheet microscopy recordings. *Scientific Reports*, 9:17625, 11 2019.

[38] Zhenzhou Wang and Haixing Li. Generalizing cell segmentation and quantification. *BMC Bioinformatics*, 18, 12 2017.

[39] Nobuyuki Otsu. A Threshold Selection Method from Gray-Level Histograms. *IEEE Transactions on Systems, Man, and Cybernetics*, 9(1):62–66, Jan 1979.

[40] Christoph Schmitz, Brian Eastwood, Susan Hendricks Tappan, Jack Glaser, Daniel Peterson, and Patrick Hof. Current automated 3D cell detection methods are not a suitable replacement for manual stereologic cell counting. *Frontiers in neuroanatomy*, 8:27, 05 2014.

[41] Casper Foldager, Jens Nyengaard, Martin Lind, and Myron Spector. A Stereological Method for the Quantitative Evaluation of Cartilage Repair Tissue. *Cartilage*, 6:123–132, 03 2014.

[42] Berrin Zuhal Altunkaynak, Emin Mehmet Önger, Muhammed Eyup Altunkaynak, Ebru Ayrancı, and Sinan Canan. A Brief Introduction to Stereology and Sampling Strategies: Basic Concepts of Stereology. *NeuroQuantology*, 10:31–43, 03 2012.

[43] Hans Jørgen G. Gundersen and Eva Bjørn Vedel Jensen. The efficiency of systematic sampling in stereology and its prediction. *Journal of microscopy*, 147 Pt 3:229–63, 1987.

[44] Ian Goodfellow, Yoshua Bengio, and Aaron Courville. *Deep Learning*. MIT Press, 2016. `http://www.deeplearningbook.org`.

[45] Zhaozheng Yin, Ryoma Bise, Mei Chen, and Takeo Kanade. Cell Segmentation in Microscopy Imagery Using a Bag of Local Bayesian Classifiers. *IEEE International Symposium on Biomedical Imaging*, pages 125–128, 01 2010.

[46] Olaf Ronneberger, Philipp Fischer, and Thomas Brox. U-Net: Convolutional Networks for Biomedical Image Segmentation. *CoRR*, abs/1505.04597, 2015.

[47] Kota Miura, Christoph Möhl, Cornelia Monzel, Simon Nørrelykke, Fabrice P. Cordelières, Perrine Paul, Thomas Pengo, Ulrike Schulze, Christian Tischer, Sébastien Tosi, and Chong Zhang. *Bioimage Data Analysis*. 01 2016.

[48] Robert Haase, Loic A. Royer, Peter Steinbach, Deborah Schmidt, Alexandr Dibrov, Uwe Schmidt, Martin Weigert, Nicola Maghelli, Pavel Tomancak, Florian Jug, and Eugene W. Myers. CLIJ: GPU-accelerated image processing for everyone. *bioRxiv*, 2019.